Electronic Supplementary Material (ESI) for Chemical Science.

Supporting Information

Identification of Pt-based Catalysts for Propane Dehydrogenation via a Probability Analysis

Shenjun Zha, Guodong Sun, Tengfang Wu, Jiubing Zhao, Zhi-Jian Zhao*, Jinlong Gong*

S1. Computational details and the models

The adsorption energy of an adsorbate, E_{ads}, was calculated as follows:

$$E_{ads} = E_{total} - E_{adsorbate} - E_{surface}$$

where E_{total} is the total energy of the slab with an attached adsorbate. $E_{adsorbate}$ is the total energy of a gas molecule. $E_{surface}$ is the total energy of a relaxed clean slab.

The surface *d*-band center (ε_d) and *d*-band width (W_d) were computed as the first and second moments of the projected *d*-band density of states. The *d*-band filling (N_d) was calculated by integrating the density of states to the Fermi level (E_f).[1] They were expressed as:

$$\varepsilon_d = \frac{\int_{-\infty}^{+\infty} \rho E dE}{\int_{-\infty}^{+\infty} \rho dE}$$

$$W_d^2 = \frac{\int_{-\infty}^{+\infty} \rho E^2 dE}{\int_{-\infty}^{+\infty} \rho dE}$$

$$N_d = \int_{-\infty}^{E_f} \rho dE$$

where ρ represents the density of states and E is the energy of state.

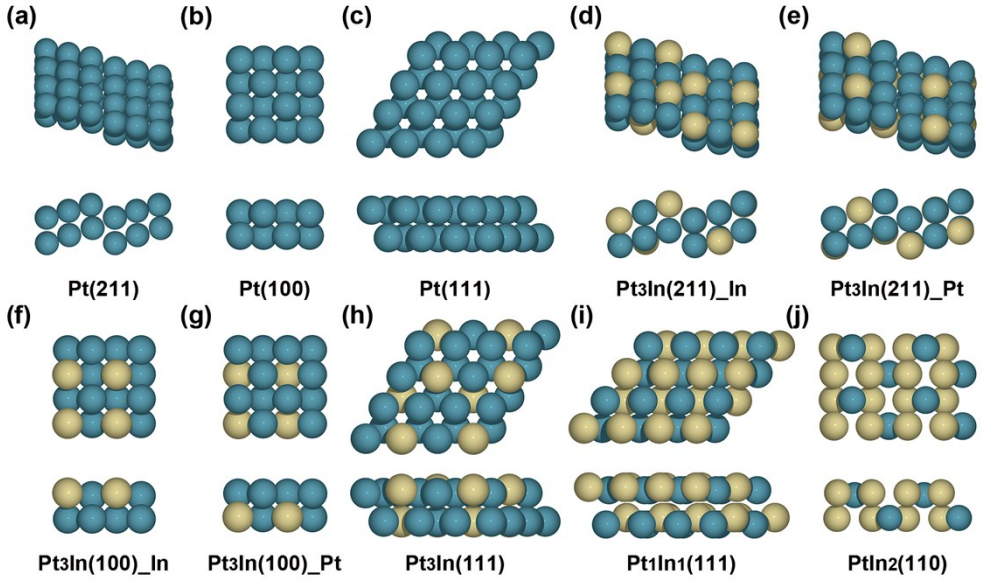

Figure S1. Top and front views of ten PtIn alloys. Pt atoms are dark blue and In atoms are light yellow.

Table S1. k-points grid and slab size of different surfaces

Surface	k-points	Slab	Surface	k-points	Slab
Pt(211)	3×2×1	3×4×4	Pt_3In(100)_In	3×3×1	2×2×4
Pt(100)	3×3×1	2×2×4	Pt_3In(100)_Pt	3×3×1	2×2×4
Pt(111)	3×3×1	4×4×4	Pt_3In(111)	3×3×1	4×4×4
Pt_3In(211)_In	3×2×1	3×4×4	Pt_1In_1(111)	3×3×1	4×4×4
Pt_3In(211)_Pt	3×2×1	3×4×4	$PtIn_2$(110)	3×3×1	6×4×4

S2. The energy profiles in screening process and the error estimation

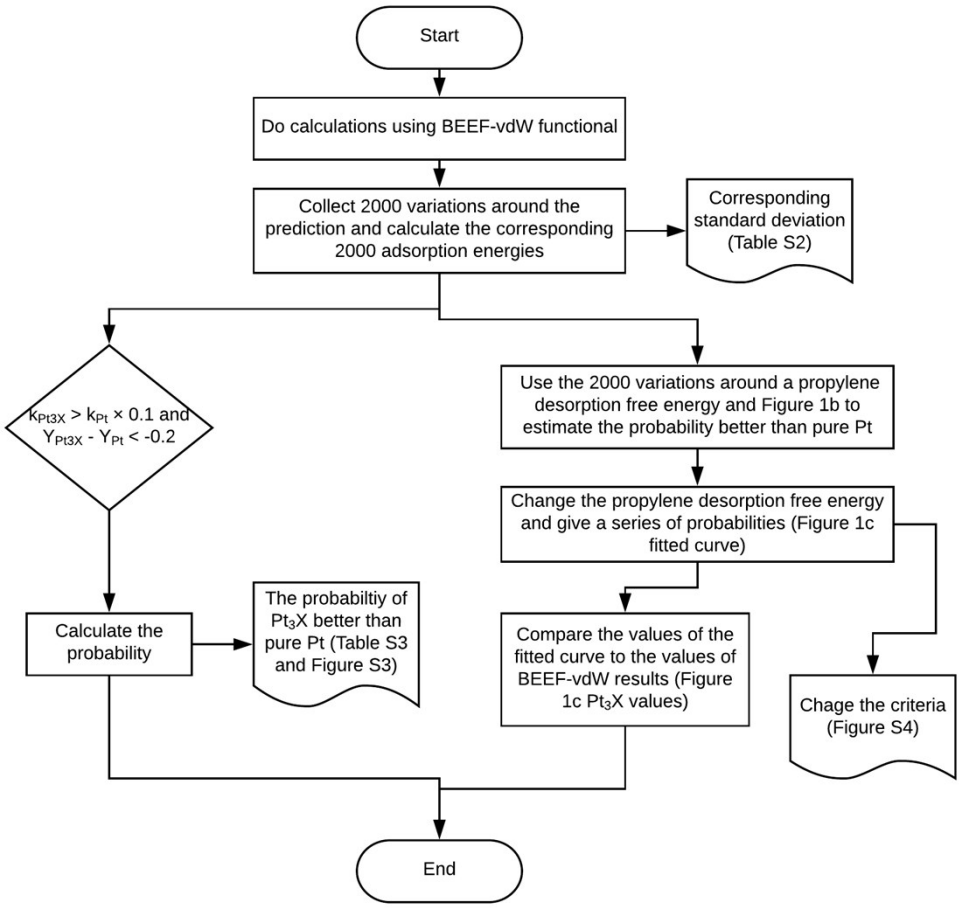

Scheme S1. The complete process of our probability analysis

Table S2. Free energy barriers of different Pt-based alloys, dehydrogenation rate constants and the corresponding standard deviation calculated by BEEF-vdW

Pt-based alloy	C_3H_8* to 1-C_3H_7* Free energy barrier/eV (Standard deviation/eV)		C_3H_8* to 1-C_3H_7* Rate constants/s^{-1}	C_3H_6* desorption Free energy barrier/eV (Standard deviation/eV)		C_3H_6* to 1-C_3H_5* Free energy barrier/eV (Standard deviation/eV)	
Pt	2.08	(0.23)	1.79×10^{1}	0.71	(0.20)	0.80	(0.30)
Pt_3Sc	2.12	(0.26)	1.05×10^{1}	0.50	(0.21)	0.80	(0.33)
Pt_3Ti	2.49	(0.24)	7.67×10^{-2}	0.14	(0.20)	0.88	(0.28)
Pt_3V	2.55	(0.23)	3.45×10^{-2}	0.13	(0.23)	1.02	(0.34)
Pt_3Cr	2.45	(0.22)	1.31×10^{-1}	0.22	(0.19)	0.96	(0.28)
Pt_3Mn	2.26	(0.23)	1.63×10^{0}	0.46	(0.20)	0.89	(0.28)
Pt_3Fe	2.14	(0.22)	8.04×10^{0}	0.62	(0.19)	0.85	(0.27)
Pt_3Co	2.10	(0.23)	1.37×10^{1}	0.68	(0.19)	0.84	(0.28)
Pt_3Ni	2.13	(0.23)	9.18×10^{0}	0.64	(0.20)	0.84	(0.29)
Pt_3Cu	2.22	(0.24)	2.78×10^{0}	0.49	(0.20)	0.87	(0.27)
Pt_3Zn	2.11	(0.23)	1.20×10^{1}	0.51	(0.19)	0.86	(0.30)
Pt_3Ga	1.74	(0.31)	1.64×10^{3}	0.82	(0.28)	0.74	(0.29)
Pt_3Y	2.19	(0.26))	4.14×10^{0}	0.45	(0.23)	0.76	(0.31)
Pt_3Zr	2.41	(0.23)	2.22×10^{-1}	0.18	(0.21)	0.88	(0.27)
Pt_3Nb	2.85	(0.27)	6.40×10^{-4}	-0.18	(0.26)	1.30	(0.27)
Pt_3Mo	2.76	(0.23)	2.12×10^{-3}	-0.13	(0.20)	1.18	(0.27)
Pt_3Tc	2.45	(0.23)	1.31×10^{-1}	0.24	(0.21)	1.00	(0.27)

Pt_3Ru	2.18	(0.23)	4.72×10^{0}	0.56	(0.20)	0.86	(0.26)
Pt_3Rh	2.07	(0.23)	2.04×10^{1}	0.72	(0.21)	0.83	(0.25)
Pt_3Pd	2.05	(0.26)	2.66×10^{1}	0.72	(0.26)	0.81	(0.26)
Pt_3Ag	2.18	(0.26)	4.72×10^{0}	0.49	(0.23)	0.82	(0.28)
Pt_3Cd	2.19	(0.25)	4.14×10^{0}	0.40	(0.22)	0.86	(0.28)
Pt_3In	2.15	(0.24)	7.04×10^{0}	0.41	(0.20)	0.86	(0.25)
Pt_3Sn	2.11	(0.22)	1.20×10^{1}	0.49	(0.20)	0.86	(0.26)

All the free energies barriers were calculated according to the reaction energies under 873K. The computational details have been provided in Section S8 and the zero-point energies have been taken into consideration.

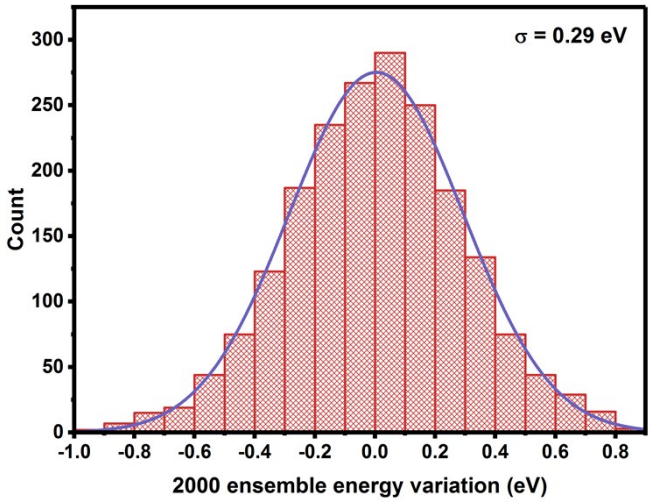

Figure S2. BEEF-vdW prediction errors for 2000 ensemble energy barriers of first dehydrogenation step of Pt_3In and the ensemble energy variation of other catalysts are all like this.

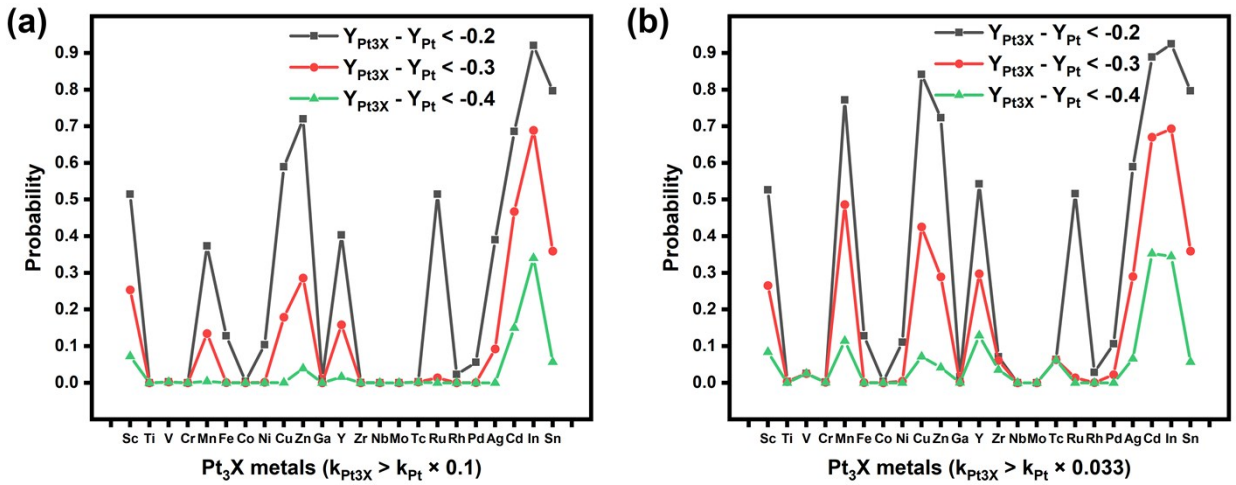

Figure S3. The probability of Pt-based catalysts better than pure Pt under a given activity ((a) $k_{Pt3X} > k_{Pt} \times 0.1$ and (b) $k_{Pt3X} > k_{Pt} \times 0.033$) and selectivity constraint condition.

Table S3. The probability of being in ideal region under different given constraint conditions

Pt-based alloy	Y_{Pt3X}-Y_{Pt}<-0.2 k_{Pt3X}>k_{Pt}×0.1	Y_{Pt3X}-Y_{Pt}<-0.3 k_{Pt3X}>k_{Pt}×0.1	Y_{Pt3X}-Y_{Pt}<-0.4 k_{Pt3X}>k_{Pt}×0.1	Y_{Pt3X}-Y_{Pt}<-0.2 k_{Pt3X}>k_{Pt}×0.033	Y_{Pt3X}-Y_{Pt}<-0.3 k_{Pt3X}>k_{Pt}×0.033	Y_{Pt3X}-Y_{Pt}<-0.4 k_{Pt3X}>k_{Pt}×0.033
Pt	0.00	0.00	0.00	0.00	0.00	0.00
Pt_3Sc	0.51	0.25	0.07	0.53	0.27	0.08
Pt_3Ti	0.00	0.00	0.00	0.00	0.00	0.00
Pt_3V	0.00	0.00	0.00	0.03	0.03	0.03
Pt_3Cr	0.00	0.00	0.00	0.00	0.00	0.00
Pt_3Mn	0.37	0.13	0.00	0.77	0.49	0.11
Pt_3Fe	0.13	0.00	0.00	0.13	0.00	0.00
Pt_3Co	0.00	0.00	0.00	0.00	0.00	0.00
Pt_3Ni	0.10	0.00	0.00	0.11	0.00	0.00
Pt_3Cu	0.59	0.18	0.00	**0.84**	0.43	0.07
Pt_3Zn	**0.72**	0.29	0.04	0.72	0.29	0.04
Pt_3Ga	0.01	0.00	0.00	0.02	0.00	0.00
Pt_3Y	0.40	0.16	0.02	0.54	0.30	0.13
Pt_3Zr	0.00	0.00	0.00	0.07	0.06	0.04
Pt_3Nb	0.00	0.00	0.00	0.00	0.00	0.00
Pt_3Mo	0.00	0.00	0.00	0.00	0.00	0.00
Pt_3Tc	0.00	0.00	0.00	0.06	0.06	0.06
Pt_3Ru	0.51	0.01	0.00	0.52	0.01	0.00
Pt_3Rh	0.02	0.00	0.00	0.03	0.00	0.00
Pt_3Pd	0.06	0.00	0.00	0.11	0.02	0.00
Pt_3Ag	0.39	0.09	0.00	0.59	0.29	0.07
Pt_3Cd	0.69	**0.47**	**0.15**	**0.89**	**0.67**	**0.35**
Pt_3In	**0.92**	**0.69**	**0.34**	**0.93**	**0.69**	**0.35**
Pt_3Sn	**0.80**	**0.36**	0.06	**0.80**	0.36	0.06

[a] Y_{Pt3X} - Y_{Pt} < -0.2 and k_{Pt3X} > k_{Pt} × 0.1 (Y: the difference of propylene desorption free energy barrier and further dehydrogenation step free energy barrier of Pt_3X, k_{Pt3X}: the rate constants of Pt_3X) mean is Pt_3X owns a better selectivity and an acceptable activity. Then, we consider Pt_3X in the acceptable region of selectivity and activity.

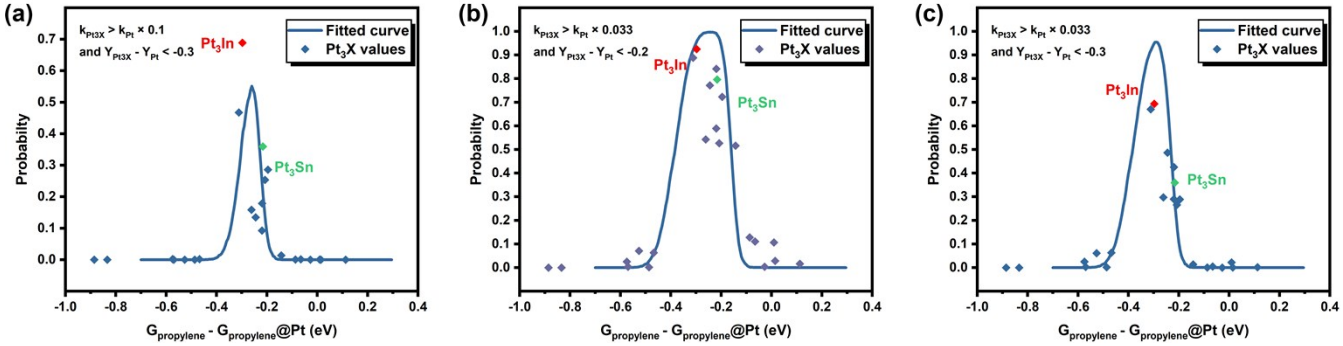

Figure S4. The probability that the activity and selectivity of a given catalyst better than pure Pt under a given activity and selectivity constraint condition as a function of propylene desorption free energy barrier relative to that of Pt ((a) Y_{Pt3X}-Y_{Pt}<-0.3 and k_{Pt3X}>k_{Pt}×0.1 (b) Y_{Pt3X}-Y_{Pt}<-0.2 and k_{Pt3X}>k_{Pt}×0.033 (c) Y_{Pt3X}-Y_{Pt}<-0.3 and k_{Pt3X}>k_{Pt}×0.033)

S3. Experimental section

All the catalysts were prepared by incipient wetness impregnation method to obtain 0.3wt % Pt loading. $H_2PtCl_6 \cdot 6H_2O$ (Chemart (Tianjin) Chemical Technology Co., Ltd., 99.9%) and $In(NO_3)_2 \cdot xH_2O$ (J&K Scientific Ltd., 99.9%) were used as precursors and SiO_2 (Alfa Aesar (China) Chemicals Co., Ltd., amorphous fumed) was used as support. After impregnation, the catalysts were dried at 80 °C for 12 h and then calcined at 600 °C for 2h. The metal loading was based on the weight ratio between metal and SiO_2.

H_2-O_2 titration measurements were carried out on a Micromeritics AutoChem II 2920 apparatus with a thermal conductive detector. For every test, 100 mg sample was pre-reduced at 600 °C with a flow rate of 30 mL min^{-1} of 10 vol% H_2/Ar for 1h, and then cooled down to 50 °C in Ar atmosphere. Subsequently, 10 vol% O_2/He was introduced to the sample by injection pulses till no visible change in the consumption peaks. And then, 10 vol% H_2/Ar was admitted to the sample by injection pulses. It can be assumed that the adsorption stoichiometry factor of Pt/H_2 was equal to 2/3. The platinum dispersion is calculated by the Eq. (1):

$$\text{Dispersion (\%)} = V_{H2} \times 2/3 \times MW_{Pt} / (W_{Pt} \times 224.14) \quad (1)$$

where V_{H2} is the volume of adsorbed H_2 (mL), MW_{Pt} is the atomic weight of Pt (g mol^{-1}), and W_{Pt} is the weight of Pt supported on the sample (g).

Catalytic measurements were performed on a quartz fixed-bed reactor (8 mm inside diameter) at 600 °C under atmosphere pressure. 250 mg of fresh catalyst (particle size of 20 to 40 mesh) was packed inside the quartz tube and heated to reaction temperature (10 °C/min) in a N_2 flow. Then, a mixture of 14 vol% propane and 14 vol% H_2 in N_2 was fed in a rate of 50 mL/min. The hydrogen cofeeding may reduce the coverage of coke precursors and change the reaction pathway.[2] The weight hourly space velocity (WHSV) of propane was 3 h^{-1}.[3] Exhaust streams were analyzed with an online GC (2060) equipped with a flame ionization detector (Chromosorb 102 column) and a thermal conductivity detector (Al_2O_3 Plot column). The propane conversion and selectivity to propylene were calculated from Eq. (2) and Eq. (3) respectively:

$$\text{Con (\%)} = ([F_{C3H8}]_{inlet} - [F_{C3H8}]_{outlet}) / [F_{C3H8}]_{inlet} \quad (2)$$

$$\text{Sel (\%)} = 100 \times n_i \times [F_{C3H6}]_{outlet} / [3 \times ([F_{C3H8}]_{inlet} - [F_{C3H8}]_{outlet})] \quad (3)$$

where i stands for different hydrocarbon products in exhaust gases, n_i is the number of carbon atom of component i, and F_i is the corresponding molar flow rate.

S4. Segregation energies, global optimization and surface energies of PtIn catalysts

Table S4. The segregation energies of PtIn catalysts

E_{seg}/eV	$Pt_3In(211)\_In$	$Pt_3In(100)\_In$	$Pt_3In(111)$	$Pt_1In_1(111)$
Our model	0.00	0.00	0.00	0.00
Pt segregation	4.15	4.14	4.63	14.02
In segregation	1.12	Not available[a]	2.97	Not converged

[a] no In in second layer available.

The segregation energies are calculated by the following equation:

$$E_{seg} = E_{surface\ alloy} - E_{bulk\ alloy}$$

where $E_{surface\ alloy}$ is the energy of surface alloy which first subsurface layer Pt or In segregates to the surface and $E_{bulk\ alloy}$ is the energy of bulk alloy which is uniform in bulk. The more positive E_{seg} is, the less stable surface alloy is.

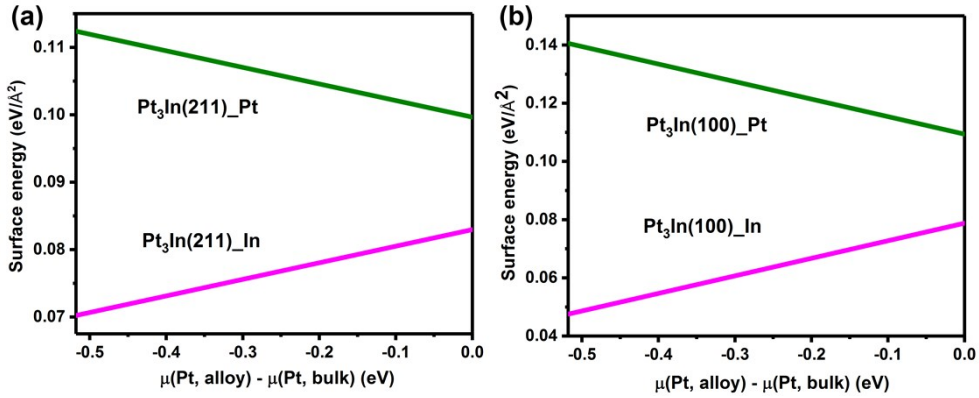

Figure S5. The surface energies of the two possible surfaces of (a) $Pt_3In(211)$ and (b) $Pt_3In(100)$.

The approach we used to calculate the surface energy is listed below.[4, 5]

The chemical potential of the bulk alloy:

$$\mu_{Pt3In}^{alloy} = 3\mu_{Pt}^{alloy} + \mu_{In}^{alloy} = 3\mu_{Pt}^{bulk} + \mu_{In}^{bulk} - \Delta H_{Pt3In}$$

where the μ_{Pt3In}^{alloy} is the chemical potential of Pt_3In alloy and represented by the chemical potentials of Pt and In in Pt_3In (μ_{Pt}^{alloy} and μ_{In}^{alloy}). They can be related to the chemical potentials of bulk Pt (μ_{Pt}^{bulk}), bulk In (μ_{In}^{bulk}) and the alloy formation enthalpy (ΔH_{Pt3In}).

The μ_{Pt}^{alloy} is in the range:

$$\mu_{Pt}^{bulk} - \frac{1}{3}|\Delta H_{Pt3In}| \le \mu_{Pt}^{alloy} \le \mu_{Pt}^{bulk}$$

Then，the surface energy can be expressed below:

$$\gamma = \frac{E_{slab} - \Delta N\mu_{Pt}^{bulk} - N_{In}\mu_{Pt3In} - \Delta N[\mu_{Pt}^{alloy} - \mu_{Pt}^{bulk}]}{2A}$$

where $\Delta N = N_{Pt} - 3N_{In}$, N_{Pt} and N_{Pt} stand for the number of Pt and In atoms in the slab, and A is the surface area of the slab in xy plane. $\mu = G = E + E_{ZPE}$, E is the energy calculated by VASP and the E_{ZPE} is the zero-point energy.

S5. Surface adsorption

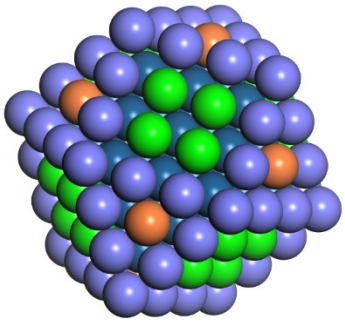

Figure S6. The scheme of simulated 1.6 nm particles. Purple: step atoms represented by (211) facets, green: (100) facets, orange: (111) facets, blue: bulk atoms.

C_3H_8 & C_3H_6

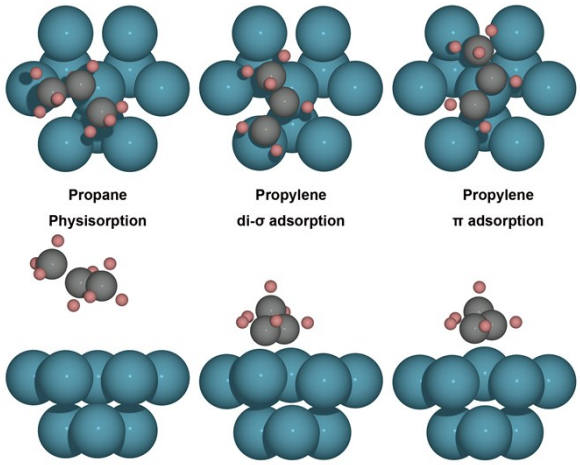

Figure S7. The physisorption of propane, di-σ and π adsorption of propylene.

Table S5. Adsorption energies of propane and propylene on different facets.

Adsorption energy/eV	Propane	Propylene	Adsorption energy/eV	Propane	Propylene
Pt(211)	-0.23	-1.37	Pt_3In(100)_In	-0.30	-0.79
Pt(100)	-0.23	-1.17	Pt_3In(100)_Pt	-0.23	-1.00
Pt(111)	-0.24	-1.10 (-1.07[a])	Pt_3In(111)	-0.23	-0.80 (-0.77[a])
Pt_3In(211)_In	-0.16	-0.87	Pt_1In_1(111)	-0.29	-0.38
Pt_3In(211)_Pt	-0.22	-1.31	$PtIn_2$(110)	-0.17	-0.23

[a] the adsorption energy of propylene co-adsorbing with a H atom.

Table S6. The adsorption energies of propylene on different surfaces with different adsorption modes (π adsorption energy modes were used as a reference)

Surface/eV	di-σ mode	π mode	C_3H_6*_cross
Pt(211)	-0.13	0	0.06
Pt(100)	-0.08	0	
Pt(111)	-0.25	0	
Pt_3In(211)_In		0	0.36
Pt_3In(211)_Pt	-0.19	0	0.14
Pt_3In(100)_In		0	
Pt_3In(100)_Pt	-0.06	0	
Pt_3In(111)	-0.13	0	
Pt_1In_1(111)	0.67	0	
$PtIn_2$(110)		0	

The adsorption energies of propane on all different surfaces calculated by BEEF-vdW functional are summarized in Table S5. Common GGA functionals are suitable for computing many important quantities in chemistry and condensed matter physics, but appear

to be unable to describe van der Waals dispersion interactions.[6] As a result, PBE and RPBE functionals offer a poor description of propane adsorption and the predicted adsorption energies are about 0.[7, 8] BEEF-vdW includes van der Waals dispersion interactions and the calculated adsorption energies are in the range of -0.30~-0.16eV, which means the adsorption of propane is physisorption and BEEF-vdW offers a better description of van der Waals dispersion interactions than PBE and RPBE.[6] The adsorption structure of propane on Pt(111) is illustrated in Figure S7 for an example and the others on different surfaces are all like that on Pt(111).

There are two main adsorption modes of propylene, di-σ and π adsorption, which are illustrated in Figure S7. From our calculated results, propylene prefers to bind to Pt atoms rather than In atoms. On Pt(211), Pt(100), Pt(111), Pt_3In(211)_Pt, Pt_3In(100)_Pt, Pt_3In(111), di-σ mode is energetically more favorable (Table S6) due to the existence of two adjacent Pt atoms. The length of C=C bond increases from 1.34 Å in gas phase to about 1.48 Å after adsorption which is the typical length of C-C bond, indicating the rehybridization of C from sp^2 to sp^3. On Pt_3In(211)_In, Pt_3In(100)_In, Pt_1In_1(111) and $PtIn_2$(110), propylene prefers π mode and the length of C=C bond is about 1.40 Å, which can be attributed to the lack of two adjacent Pt atoms or the too large distance between two Pt atoms (Pt_1In_1(111)). Therefore, one of the geometric effect of In can be attributed to the separation of adjacent Pt atoms, which leads to the transformation from di-σ adsorption mode to π adsorption mode and the decrement of propylene adsorption energy.

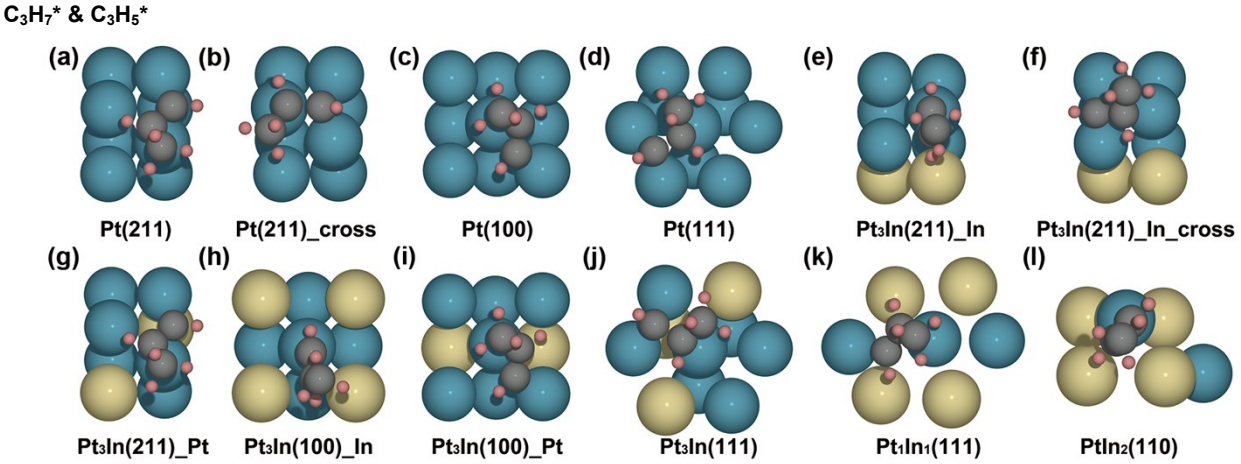

Figure S8. Adsorption geometries of 1-C_3H_5* on different PtIn alloy surfaces

On all surfaces, both C_3H_7* and C_3H_5* only tend to bind with the Pt atoms. More importantly, it must be noted all the C_3H_5* prefer to only interact with the step Pt atoms on (211) facets (Figure S8), which ensures the intermediates on (211) facets discussed below all interact with the step Pt atoms.

On all surfaces, both 1-C_3H_7* and 2-C_3H_7* tend to adsorb to only one surface Pt atom on the top site. C_3H_5* lost three H atoms and tend to bind to three metal atoms intuitively. On Pt(211) and Pt_3In(211)_Pt, 1-C_3H_5* and 2-C_3H_5* prefers binding to only two step Pt atoms (Figure S8a and g) rather than bind to two step Pt atoms and one terrace Pt atom (Figure S8b). The bond length of C=C increases from 1.34 Å to 1.41 Å, which means the breakage of C=C and the formation of three σ-like bond. On Pt_3In(211)_In, the step sites are arrayed by Pt and In atom one by one. 1-C_3H_5* and 2-C_3H_5* tend to bind to only one step Pt atom in a σ-like mode (Figure S8e) rather than bind to one step and two terrace Pt atoms (Figure S8f). The bond length of C=C is still 1.34 Å just as that of propylene. This indicates that it won't break the C=C of C_3H_5* on Pt_3In(211)_In. On Pt(100), Pt_3In(100)_Pt and Pt_1In_1(111) (Figure S8c, i and k), due to the lack of three adjacent Pt atoms, 1-C_3H_5* and 2-C_3H_5* tend to bind to two Pt atoms, just like on Pt_3In(211)_Pt. On Pt(111) and Pt_3In(111) (Figure S8d and j), 1-C_3H_5* and 2-C_3H_5* prefer binding to three Pt adjacent atoms in σ-like mode. On Pt_3In(100)_In and $PtIn_2$(110) (Figure S8h and l), 1-C_3H_5* and 2-C_3H_5* tend to bind to only one Pt atom, due to the lack of two adjacent Pt atoms.

S6. Potential energy profiles of different routes

Table S7. Potential energy profiles of different routes

Potential energy/eV	Pt(211)	Pt(100)	Pt(111)	$Pt_3In(211)\_In$	$Pt_3In(211)\_Pt$
$C_3H_8(g)\rightarrow 1\text{-}C_3H_8^*$	-0.23	-0.23	-0.24	-0.16	-0.22
$C_3H_8^*\rightarrow 1\text{-}C_3H_7^*$ (TS)	0.69	0.76	0.95	0.81	0.91
$C_3H_8^*\rightarrow 2\text{-}C_3H_7^*$ (TS)	0.62	0.71	1.03	0.89	0.74
$1\text{-}C_3H_7^*\rightarrow C_3H_6^*$ (TS)	0.55	0.69	0.87	0.92	0.57
$2\text{-}C_3H_7^*\rightarrow C_3H_6^*$ (TS)	0.51	0.73	0.93	0.57	0.59
$C_3H_6^*\rightarrow 1\text{-}C_3H_5^*$ (TS)	0.54	0.74	0.96	1.19	0.63
$C_3H_6^*\rightarrow 2\text{-}C_3H_5^*$ (TS)	0.53	0.92	0.99	1.14	0.71
$C_3H_6^*\rightarrow C_3H_6(g)$	-1.37	-1.17	-1.10	-0.87	-1.31
Potential energy/eV	$Pt_3In(100)\_In$	$Pt_3In(100)\_Pt$	$Pt_3In(111)$	$Pt_1In_1(111)$	$PtIn_2(110)$
$C_3H_8(g)\rightarrow 1\text{-}C_3H_8^*$	-0.30	-0.23	-0.23	-0.29	-0.17
$C_3H_8^*\rightarrow 1\text{-}C_3H_7^*$ (TS)	1.15	0.81	1.00	1.93	1.75
$C_3H_8^*\rightarrow 2\text{-}C_3H_7^*$ (TS)	1.14	0.76	1.43		1.75
$1\text{-}C_3H_7^*\rightarrow C_3H_6^*$ (TS)	1.24	0.64	0.92	1.17	1.47
$2\text{-}C_3H_7^*\rightarrow C_3H_6^*$ (TS)	1.28	0.65	0.86		1.40
$C_3H_6^*\rightarrow 1\text{-}C_3H_5^*$ (TS)	1.25	0.71	1.02	1.42	1.44
$C_3H_6^*\rightarrow 2\text{-}C_3H_5^*$ (TS)	1.30	0.83	0.99		1.52
$C_3H_6^*\rightarrow C_3H_6(g)$	-0.79	-1.00	-0.80	-0.38	-0.23

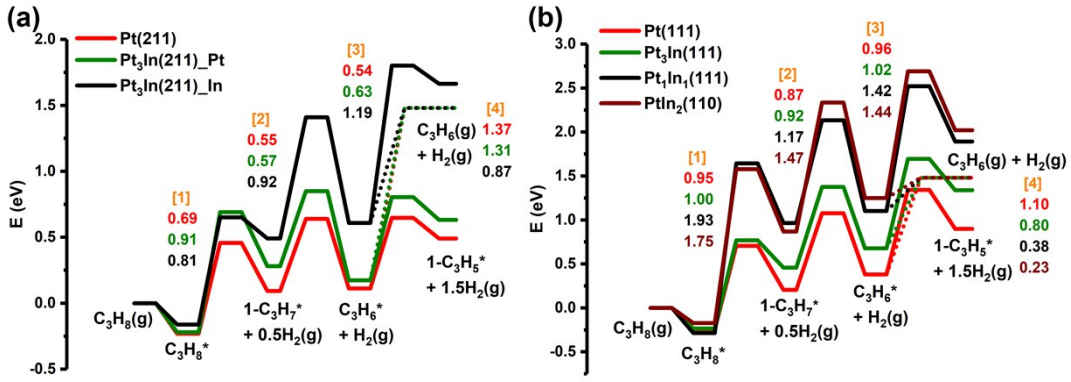

Figure S9. Potential energy diagram (a) α-type PDH reaction on Pt(211), $Pt_3In(211)\_Pt$ and $Pt_3In(211)\_In$. (b) α-type PDH reaction on Pt(111), $Pt_3In(111)$, Pt_1In_1 (111) and $PtIn_2(110)$.

From the view of potential energy (Figure S9), the energy profiles of the dominating (211) facets were compared first. The first dehydrogenation energy barrier of Pt(211) is 0.69 eV, while $Pt_3In(211)\_Pt$ (0.91 eV) and $Pt_3In(211)\_In$ (0.81 eV) have a little higher activation energies. This implies the energy barrier increases with the addition of In, i.e. In decreases the activity of PDH reaction. Pt(211) and $Pt_3In(211)\_Pt$ have a similar further dehydrogenation barrier from $C_3H_6^*$ to $1\text{-}C_3H_5^*$ (0.54 eV and 0.63 eV) which is much lower than the desorption energy of $C_3H_6^*$ (1.37 eV and 1.31 eV), indicating $Pt_3In(211)\_Pt$ will not improve the poor selectivity of Pt(211).[9] However, The further dehydrogenation barrier of $Pt_3In(211)\_In$ (1.19 eV) is much higher than the desorption energy of $C_3H_6^*$ (0.87 eV), which means $Pt_3In(211)\_In$ will greatly improve the selectivity to propylene. Because the properties of two possible surfaces of $Pt_3In(211)$ may vary greatly, the surface energies of the two possible surfaces of $Pt_3In(211)$ were calculated to obtain a more thermodynamically stable surface.[4, 5] From Figure S5a, it can be observed that $Pt_3In(211)\_In$ has lower surface energies in the whole possible range, which means $Pt_3In(211)\_In$ is preferred thermodynamically. This result indicates the undercoordinated sites of Pt tend be partially covered by In atoms and plays a crucial role in elucidating the improvements in propylene selectivity. The results of Pt(100), $Pt_3In(100)\_Pt$ and $Pt_3In(100)\_In$ are similar to (211) facets mentioned above (Table S7).

To elucidate the relationship between the ratio of In and reaction activity, the potential energies on Pt(111), $Pt_3In(111)$, $Pt_1In_1(111)$ and $PtIn_2(110)$ were also compared. The first dehydrogenation barrier of Pt(111) (0.95 eV) and $Pt_3In(111)$ (1.00 eV) are almost the same. When the PtIn ratio comes to 1:1 and 1:2, the first dehydrogenation energy barrier has an obvious increase (1.93 eV and 1.75 eV). This means the activity will suffer a great loss when the PtIn ratio is higher than 3:1, When it comes to selectivity, the desorption energy barrier of propylene is higher than propylene further dehydrogenation barrier on Pt(111), which corresponds to the selectivity problem of pure Pt catalyst that propylene tend to further dehydrogenation rather than desorption. With the addition of In, $Pt_3In(111)$,

Pt_1In_1(111) and $PtIn_2$(111) all have a lower propylene desorption energy barrier than that of further dehydrogenation. Although Pt_1In_1(111) and $PtIn_2$(110) have an obviously higher further dehydrogenation barrier than Pt_3In(111) which means a better selectivity, their reaction activity is much lower and the improvements in selectivity are hard to compensate for the great loss of activity.

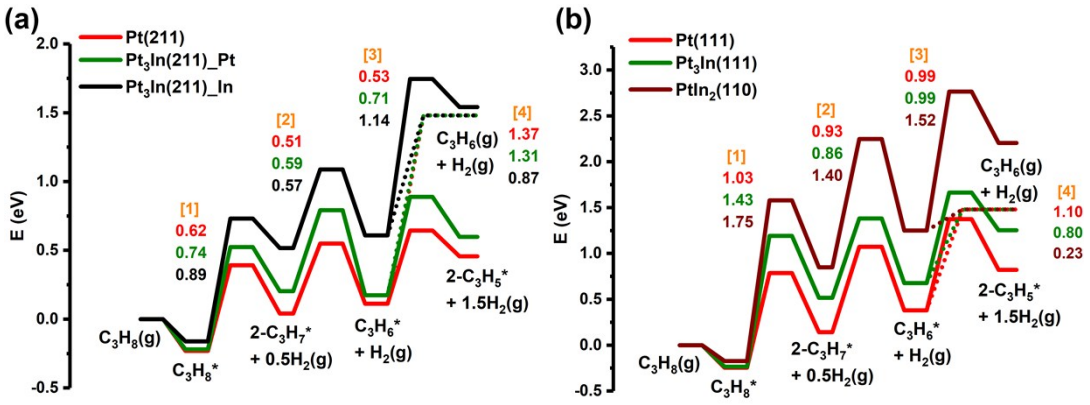

Figure S10. Potential energy diagram (a) β-type PDH reaction on Pt(211), Pt_3In(211)_Pt and Pt_3In(211)_In. (b) β-type PDH reaction on Pt(111), Pt_3In(111), Pt_1In_1(111) and $PtIn_2$(110).

The route of β-type PDH reaction (from C_3H_8* to 2-C_3H_7* to C_3H_6* to 2-C_3H_5*) has the similar trends to α-type PDH reaction (Figure S10).

In summary, a Pt_3In cluster which contains Pt_3In(211)_In, Pt_3In(100)_In and Pt_3In(111) have a similar activity to a pure Pt cluster, while the clusters which own higher In ratio have a great loss in activity. Furthermore, the addition of In can improve the selectivity of pure Pt cluster. In other words, a Pt_3In cluster may finally have the largest propylene formation performance.

S7. Free energy profiles of different routes

Table S8. Free energy profiles of different routes

Free energy/eV	Pt(211)	Pt(100)	Pt(111)	$Pt_3In(211)\_In$	$Pt_3In(211)\_Pt$
$C_3H_8(g)\rightarrow 1\text{-}C_3H_7^*$ (TS)	1.84	1.91	2.08	2.05	2.08
$C_3H_8(g)\rightarrow 2\text{-}C_3H_7^*$ (TS)	1.78	1.85	2.16	2.12	1.91
$1\text{-}C_3H_7^*\rightarrow C_3H_6^*$ (TS)	0.30	0.42	0.63	0.67	0.33
$2\text{-}C_3H_7^*\rightarrow C_3H_6^*$ (TS)	0.29	0.47	0.68	0.33	0.37
$C_3H_6^*\rightarrow 1\text{-}C_3H_5^*$ (TS)	0.41	0.60	0.80	1.02	0.50
$C_3H_6^*\rightarrow 2\text{-}C_3H_5^*$ (TS)	0.40	0.76	0.84	0.96	0.57
$C_3H_6^*\rightarrow C_3H_6(g)$	-0.15	-0.35	-0.43	-0.66	-0.21
Free energy/eV	$Pt_3In(100)\_In$	$Pt_3In(100)\_Pt$	$Pt_3In(111)$	$Pt_1In_1(111)$	$PtIn_2(110)$
$C_3H_8(g)\rightarrow 1\text{-}C_3H_7^*$ (TS)	2.27	1.95	2.15	3.04	2.96
$C_3H_8(g)\rightarrow 2\text{-}C_3H_7^*$ (TS)	2.24	1.89	2.57		2.96
$1\text{-}C_3H_7^*\rightarrow C_3H_6^*$ (TS)	0.99	0.36	0.61	0.85	1.14
$2\text{-}C_3H_7^*\rightarrow C_3H_6^*$ (TS)	1.03	0.38	0.58		1.14
$C_3H_6^*\rightarrow 1\text{-}C_3H_5^*$ (TS)	1.07	0.57	0.86	1.27	1.29
$C_3H_6^*\rightarrow 2\text{-}C_3H_5^*$ (TS)	1.12	0.67	0.83		1.36
$C_3H_6^*\rightarrow C_3H_6(g)$	-0.75	-0.51	-0.73	-1.13	-1.27

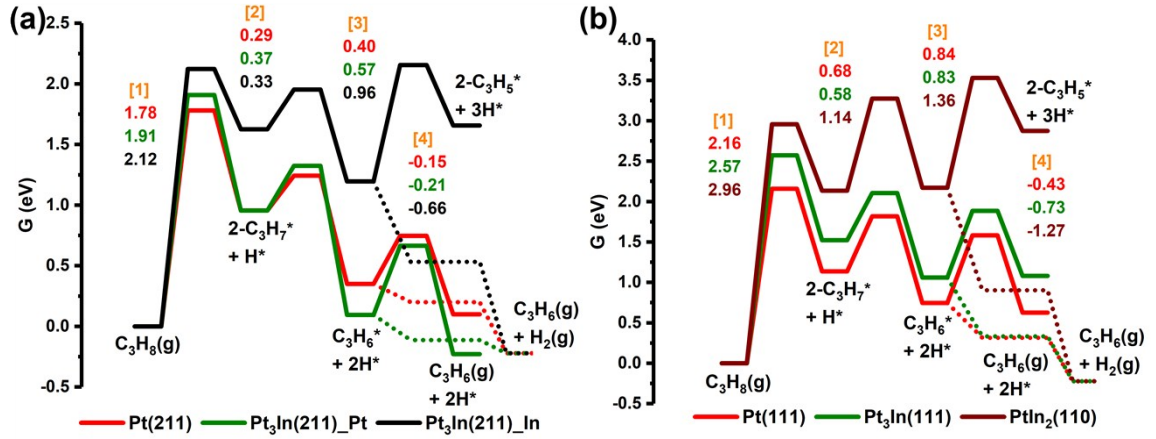

Figure S11. Gibbs free energy diagram (a) β-type PDH reaction on Pt(211), $Pt_3In(211)\_Pt$ and $Pt_3In(211)\_In$. (b) β-type PDH reaction on Pt(111), $Pt_3In(111)$, and $PtIn_2(110)$

Due to the deficient performance of harmonic approximation for estimating the entropy of adsorbed species, the entropies were calculated based on the empirical equation suggested by Campbell et al. [10, 11]:

$$S_{ad}^{0}(T) = S_{gas}^{0}(T) - 3.3R$$

where S_{ad}^{0} and S_{gas}^{0} are the entropies of adsorbate and gas molecules and *R* is the ideal gas constant. For a surface reaction, the entropy change was ignored. It must be pointed out the analysis proposed by Campbell et al. only corresponds to terrace sites and should be carefully applied to defect sites.[10]

The adsorption mode of propane was not taken into consideration in free energy analysis. The adsorption mode of propane is physisorption on the surface which makes it hard to identify the entropy of propane.

S8. A mean field microkinetic analysis

A mean field microkinetic analysis was performed by our own microkinetic simulation program.[12] The model was developed based on the DFT-obtained thermodynamic and kinetic data from all elementary steps and the experimental reaction conditions (T = 873K, feed composition: C_3H_8 = 20%, H_2 = 25%). The rate constants were calculated based on the transition state theory (TST):

$$k = \frac{k_B T}{h} e^{-\frac{\Delta G^{\neq}}{k_B T}}$$

where k is the rate constant of an elementary reaction step, $\Delta G^{\neq}$ is the Gibbs activation energy, k_B is the Boltzmann constant and T is the reaction temperature.

In the microkinetic modeling, the steady state is calculated by a time integration method until a steady surface coverage and product pressure are reached.[12] The rate at time t of each individual step is calculated, according to the partial pressure and surface coverage of each species at that time. The new partial pressure or surface coverage for species c at time $t+\Delta t$ is calculated following the formula below:

$$\theta_c(t+\Delta t) = \theta_c(t) + \Delta\theta_c = \theta_c(t) + \int_t^{t+\Delta t} \frac{d\theta_c}{dt} = \theta_c(t) + r_c \Delta t$$

where t is time, Δt is time step which is used in the integration, θ_c (t) is the coverage of species c at time t and r_c is the total reaction rate of species c.

The rate-controlling steps was identified via calculating the "Degree of Rate Control" introduced by Campbell et al.[13-15]:

$$X_{RC,i} = \frac{k_i}{r}\left(\frac{\partial r}{\partial k_i}\right)_{k_{j\neq i}, K_i} = \left(\frac{\partial In(r)}{\partial In(k_i)}\right)_{k_{j\neq i}, K_i}$$

where r is the reaction rate and k is the rate constants. The degree of rate control is calculated in our kinetic model by increasing both the forward and reverse rate constants by 1% for the elementary reactions, which won't change the equilibrium.

Adsorbates on an ordered surface attempt to minimize their free energy when moving on the surface, which is difficult to treat exactly.[16] Thus, basic assumptions of our kinetic model were introduced:

1. Surface is homogeneous (For PtIn alloys, only the Pt active sites were taken into consideration)
2. All Pt sites are equivalent
3. Each site can hold at most one adsorbate
4. There are no interactions between adsorbates

In this microkinetic modeling, three types of free molecules, seven surface species and eight elementary steps were included. The temperature was set as 873K and pressure was set to $P_{C3H8(g)}$ = 0.2 and $P_{H2(g)}$ = 0.25. The rate equations of all surface species are as follows:

$$r_{C3H8(g)} = \frac{d\theta_{C3H8(g)}}{dt} = -r1 - r2 \quad (1)$$

$$r_{C3H6(g)} = \frac{d\theta_{C3H6(g)}}{dt} = +r7 \quad (2)$$

$$r_{H2(g)} = \frac{d\theta_{H2(g)}}{dt} = +r8 \quad (3)$$

$$r_{1-C3H7*} = \frac{d\theta_{1-C3H7*}}{dt} = -r3 + r1 \quad (4)$$

$$r_{2-C3H7*} = \frac{d\theta_{2-C3H7*}}{dt} = -r4 + r2 \quad (5)$$

$$r_{C3H6*} = \frac{d\theta_{C3H6*}}{dt} = -r5 - r6 - r7 + r3 + r4 \quad (6)$$

$$r_{1-C3H5*} = \frac{d\theta_{1-C3H5*}}{dt} = +r5 \quad (7)$$

$$r_{2-C3H5*} = \frac{d\theta_{2-C3H5*}}{dt} = +r6 \quad (8)$$

$$r_{H*} = \frac{d\theta_{H*}}{dt} = -r8 - r8 + r1 + r2 + r3 + r4 + r5 + r6 \quad (9)$$

The coke formation was not explicitly included in our micro-kinetic modeling. The simplification of our reaction network in the micro-kinetic modelling is mainly due to the following reasons: (1) the coke formation mechanism is very complex, which is also not the main focus of our study. (2) the formation of C_3H_5* is just used as a model precursor for coke formation, which seems to be widely accepted by previous studies C-C bond breaking needs deeply dehydrogenated precursor, i.e. propyne (CH_3CCH*), which means the 1-C_3H_5* (CH_3CHCH*) can be viewed as the origin of deeply dehydrogenated species and coke precursors.[4, 8]

Table S9. List of PDH rate (molC_3H_6 molsite^{-1} s^{-1}) of elementary steps

	List of reactions	Reaction rate
R1	$C_3H_8(g) + * \rightleftharpoons 1-C_3H_7* + H*$	$r_1 = k_1 P_{C3H8(g)}\theta_v - k_{-1}\theta_{1-C3H7*}\theta_{H*}$
R2	$C_3H_8(g) + * \rightleftharpoons 2-C_3H_7* + H*$	$r_2 = k_2 P_{C3H8(g)}\theta_v - k_{-2}\theta_{2-C3H7*}\theta_{H*}$
R3	$1-C_3H_7* + * \rightleftharpoons C_3H_6* + H*$	$r_3 = k_3\theta_{1-C3H7*}\theta_v - k_{-3}\theta_{C3H6*}\theta_{H*}$
R4	$2-C_3H_7* + * \rightleftharpoons C_3H_6* + H*$	$r_4 = k_4\theta_{2-C3H7*}\theta_v - k_{-4}\theta_{C3H6*}\theta_{H*}$
R5	$C_3H_6* + * \rightleftharpoons 1-C_3H_5* + H*$	$r_5 = k_5\theta_{C3H6*}\theta_v - k_{-5}\theta_{1-C3H5*}\theta_{H*}$
R6	$C_3H_6* + * \rightleftharpoons 2-C_3H_5* + H*$	$r_6 = k_6\theta_{C3H6*}\theta_v - k_{-6}\theta_{2-C3H5*}\theta_{H*}$
R7	$C_3H_6* \rightleftharpoons C_3H_6(g) + *$	$r_7 = k_7\theta_{C3H6*} - k_{-7}P_{C3H6}\theta_v$
R8	$H* + H* \rightleftharpoons H_2(g) + 2*$	$r_8 = k_8\theta_{H*}^2 - k_{-8}P_{H2}\theta_v^2$

Table S10. Coverage of reaction intermediate

Surface	1-C_3H_7*	2-C_3H_7*	C_3H_6*	1-C_3H_5*	2-C_3H_5*	H*	*
Pt(211)	2.57 × 10^{-10}	5.00 × 10^{-10}	1.49 × 10^{-11}	7.93 × 10^{-09}	1.35 × 10^{-08}	2.98 × 10^{-02}	0.970
Pt(100)	5.00 × 10^{-10}	2.16 × 10^{-09}	6.00 × 10^{-12}	1.26 × 10^{-09}	2.79 × 10^{-09}	1.05 × 10^{-02}	0.990
Pt(111)	8.51 × 10^{-10}	5.71 × 10^{-10}	2.61 × 10^{-13}	3.67 × 10^{-11}	9.30 × 10^{-11}	1.36 × 10^{-02}	0.986
Pt_3In(211)_In	2.03 × 10^{-09}	9.27 × 10^{-12}	3.89 × 10^{-13}	5.10 × 10^{-14}	2.52 × 10^{-13}	3.41 × 10^{-03}	0.996
Pt_3In(100)_In	4.81 × 10^{-09}	8.12 × 10^{-09}	1.82 × 10^{-14}	3.56 × 10^{-15}	3.12 × 10^{-15}	1.28 × 10^{-02}	0.987
Pt_3In(111)	2.56 × 10^{-10}	6.50 × 10^{-13}	7.64 × 10^{-14}	1.37 × 10^{-12}	4.53 × 10^{-12}	1.28 × 10^{-02}	0.987
Pt_1In_1(111)	4.55 × 10^{-14}		5.64 × 10^{-19}	1.05 × 10^{-18}		1.29 × 10^{-05}	1.000

The rate-controlling steps was identified via calculating the "Degree of Rate Control" introduced by Campbell et al.[13-15]:

$$X_{RC,i} = \frac{k_i}{r}\left(\frac{\partial r}{\partial k_i}\right)_{k_{j\neq i}, K_i} = \left(\frac{\partial In(r)}{\partial In(k_i)}\right)_{k_{j\neq i}, K_i}$$

where *r* is the reaction rate and *k* is the rate constants. The degree of rate control is calculated in our kinetic model by increasing both the forward and reverse rate constants by 1% for the elementary reactions, which won't change the equilibrium.

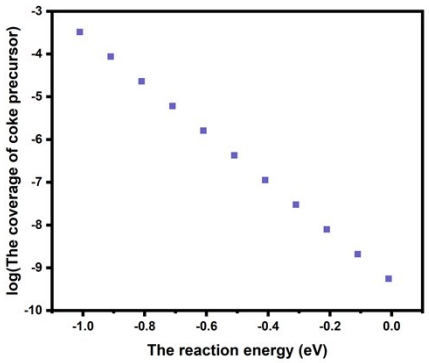

Figure S12 The relationship between the reaction energy from C_3H_6* to our model coke precursor (1-C_3H_5*) and the coverage of coke precursor on Pt(211).

For the coverage of our model coke precursor (1-C_3H_5* that has a thermodynamic equilibrium with C_3H_6* at steady state), it changed with the adsorption energy of 1-C_3H_5*.

S9. Correlation between ε_d^W and propylene π adsorption energy

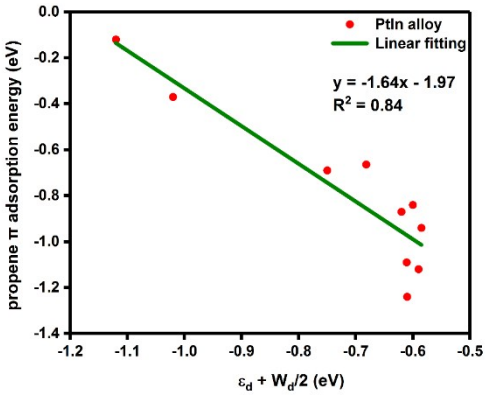

Figure S13. Correlation between ε_d^W and propylene π adsorption energy

A slight modification has been identified to improve the *d*-band center descriptor. Vojvodic et al. introduced an alternative descriptor $\varepsilon_d^W = \varepsilon_d + W_d/2$. This model explicitly explains how the bond strength depends on the anti-bonding state formed between adsorbate and metal through the upper-edge position of the *d*-states. This descriptor not only takes the average energy of *d*-band into consideration but also utilizes the information in the *d*-band width. The introduction of a width dependence ensures correlations with the upper band-edge position and hence the bond strength[17]. ε_d^W was found to be a better descriptor than *d*-band center.

Reference

1. S. D. Miller and J. R. Kitchin, *Surf. Sci.*, 2009, **603**, 794-801.
2. S. Saerens, M. K. Sabbe, V. V. Galvita, E. A. Redekop, M.-F. Reyniers and G. B. Marin, *ACS Catal.*, 2017, **7**, 7495-7508.
3. T. Wang, F. Jiang, G. Liu, L. Zeng, Z. Zhao and J. Gong, *AIChE J.*, 2016, **62**, 4365-4376.
4. L. Nykänen and K. Honkala, *ACS Catal.*, 2013, **3**, 3026-3030.
5. N. Moll, A. Kley, E. Pehlke and M. Scheffler, *Phys Rev B Condens Matter*, 1996, **54**, 8844-8855.
6. J. Wellendorff, K. T. Lundgaard, A. Møgelhøj, V. Petzold, D. D. Landis, J. K. Nørskov, T. Bligaard and K. W. Jacobsen, *Phys. Rev. B*, 2012, **85**, 235149.
7. L. Nykänen and K. Honkala, *J. Phys. Chem. C*, 2011, **115**, 9578-9586.
8. M.-L. Yang, Y.-A. Zhu, X.-G. Zhou, Z.-J. Sui and D. Chen, *ACS Catal.*, 2012, **2**, 1247-1258.
9. M. L. Yang, Y. A. Zhu, C. Fan, Z. J. Sui, D. Chen and X. G. Zhou, *Phys. Chem. Chem. Phys.*, 2011, **13**, 3257-3267.
10. C. T. Campbell and J. R. Sellers, *J. Am. Chem. Soc.*, 2012, **134**, 18109-18115.
11. C. T. Campbell, L. Árnadóttir and J. R. Sellers, *Z. Phys. Chem.*, 2013, **227**, 1435-1454.
12. Z.-J. Zhao, Z. Li, Y. Cui, H. Zhu, W. F. Schneider, W. N. Delgass, F. Ribeiro and J. Greeley, *J. Catal.*, 2017, **345**, 157-169.
13. C. T. Campbell, *Top. Catal.*, 1994, **1**, 353-366.
14. C. Stegelmann, A. Andreasen and C. T. Campbell, *J. Am. Chem. Soc.*, 2009, **131**, 8077-8082.
15. C. T. Campbell, *ACS Catal.*, 2017, **7**, 2770-2779.
16. K. Jens, F. Studt, F. Abild-Pedersen and T. Bligaard, *Fundamental concepts in heterogeneous catalysis*, John Wiley & Sons, 2014.
17. A. Vojvodic, J. K. Nørskov and F. Abild-Pedersen, *Top. Catal.*, 2013, **57**, 25-32.